





On-board Volcanic Eruption Detection through CNNs and Satellite Multispectral Imagery

Maria Pia Del Rosso , Alessandro Sebastianelli , Dario Spiller ,
Pierre Philippe Mathieu, Silvia Liberata Ullo 

Abstract—In recent years, the growth of Machine Learning algorithms in a variety of different applications has raised numerous studies on the applicability of these algorithms in real scenarios. Among all, one of the hardest scenarios, due to its physical requirements, is the aerospace one. In this context, the authors of this work aim to propose a first prototype and a study of feasibility for an AI model to be 'loaded' on board. As case study, the authors decided to investigate the detection of volcanic eruptions as a method to swiftly produce alerts. Two Convolutional Neural Networks have been proposed and created, also showing how to correctly implement them on a real hardware and how the complexity of a CNN can be adapted to fit computational requirements.

Index Terms—On-board AI, Deep Learning, Image Classification, Sentinel-2, Multispectral, Raspberry, Movidius

I. INTRODUCTION

IN recent years, Remote Sensing has seen its maximum expanse in terms of applicability and use cases. The extremely large availability of remote-sensed images, satellite-based in particular, has made many scientists approached Remote Sensing from different fields of research. A notable example is the increasing use of this type of data in Earth science and geological fields for monitoring parameters which by their nature are or may become difficult to measure, or that need a lot of time and efforts to be recorded with classical instruments. The ultimate frontier of satellite Remote Sensing which has seen once again the European Space Agency (ESA) be the pioneer in moving the first steps is represented by the use of Artificial Intelligence (AI) on-board satellites for land classification and hazards' detection.

The aim of this study is to investigate the possibility of using satellite images to monitor hazardous events by means of AI techniques and on-board computing resources [1]. The results achieved for the classification of volcanic eruptions could be suitable for future missions of the ϕ - *sat* program that represent the first experiment carried out by ESA to demonstrate how AI on-board the satellites can be used for Earth observation [2].

Many researches in the literature made use of satellite images, and Synthetic Aperture Radar (SAR) data in particular, to monitor ground movements in the proximity of a volcano's crater just before the eruption. Yet, in recent years, many

scientists have switched from classical to AI techniques as for example in [3], where the authors investigated the use of two different Deep Neural Networks (DNNs) together with a combined feature vector of linear prediction coefficients and statistical properties, for seismic events classification purposes. Similar approaches can be found using both real [4] and simulated [5] [6] Interferometric SAR (InSAR) data.

II. DATASET

Our work has focused on the volcanic eruptions and the first necessary step has consisted in building the right dataset by retrieving the data from an online database. Since no ready-to-use dataset was found to perfectly fit the specific task of this work, a specific dataset was built using an online catalog volcanic events including geolocalization information [7]. Satellite images acquired for the place and the date of the events were collected and a labeled using the open-access Python tool presented in [8].

A. The volcanic eruptions catalog

The dataset has been created by selecting the most recent volcanic eruptions reported in the Volcanoes of the World (VOTW) catalog by the Global Volcanism Program of the Smithsonian Institution: a catalog of Holocene and Pleistocene volcanoes and eruptions from the past 10,000 years [7]. An example of information available in the catalog is reported in Table I.

Eruption Start Time	Volcano name	Latitude	Longitude
2019-06-26	Ulawun	-5.050	151.330
2019-06-24	Ubinas	-16.355	151.330
2019-06-22	Raikoke	48.292	153.250
2019-06-11	Piton de la Fournaise	-21.244	55.708
2019-06-01	Great Sitkin	52.076	-176.130

TABLE I: Sample from the catalog

Since the goal is to create a set of images, the only useful information are the starting date of the eruption, the geographic coordinates and the volcano name, so these information were extracted and stored apart.

The images used to create the dataset have been collected using Landsat 7 and Sentinel 2 products, stored in Google Earth Engine [9]. Specifically, Landsat 7 images have been downloaded considering the period 1999 - 2015, whereas Sentinel 2 images are related to the period 2015 - 2019.

It is worth to highlight that there are some differences between Sentinel-2 and Landsat-7, in terms of spatial resolution and wavelength and bandwidth for the bands of interest (Table

A. Sebastianelli, M. P. Del Rosso and S. L. Ullo are with the Engineering Department, University of Sannio, Benevento, Italy, email: sebastianelli, mariapia.delrosso, ullo@unisannio.it

D. Spiller and P. P. Mathieu are with the European Space Agency, Φ -lab, Frascati, Italy, email: {dario.spiller, pierre.philippe.mathieu}@esa.int

II and Table III). These differences are addressed in the next sections.

Band name	Description	Wavelength (nm)	Bandwidth (nm)	Spatial resolution (m)
B1	Blue	485	70	30
B2	Green	560	80	30
B3	Red	660	70	30
B5	SWIR 1	1650	200	30
B7	SWIR 2	2220	260	30

TABLE II: Description of Landsat 7 bands

Band name	Description	Wavelength (nm)	Bandwidth (nm)	Spatial resolution (m)
B2	Blue	496.6 (S2A) / 492.1 (S2B)	66	10
B3	Green	560 (S2A) / 559 (S2B)	36	10
B4	Red	664.5 (S2A) / 665 (S2B)	31	10
B11	SWIR 1	1613.7 (S2A) / 1610.4 (S2B)	91 (S2A) / 94 (S2B)	20
B12	SWIR 2	2202.4 (S2A) / 2183.7 (S2B)	175 (S2A) / 185 (S2B)	20

TABLE III: Description of Sentinel 2 bands.

B. Data Preparation and Manipulation

Satellite data has been downloaded with the above mentioned tool [8], that allows to download small patches of images. In this case, $7.5km^2$ patches have been downloaded.

After downloading the data, some post-processing procedures have been applied. Firstly, the image are resized to 512×512 using the Bicubic Interpolation of Python OpenCV. This procedure mitigates the difference of spatial resolution between Sentinel-2 and Landsat-7. Secondly, infrared bands are combined with RGB bands, in order to highlight the color of the volcanic lava, that, after an initial state, gets darker, even though its temperature is very high. In order to highlight this feature a temperature sensitive band, like the infrared ones, have been used. Moreover, the proposed algorithm has been used in the experimental phase with a Raspberry PI and camera, and since the PI camera acquires only RGB data, in order to simulate a realistic eruption the bands combination became necessary. The bands combination for IR highlighting is given by equation:

$$RED = \alpha_1 \cdot B4 + \max(0, B12 - 0.1) \quad (1a)$$

$$GREEN = \alpha_1 \cdot B3 + \max(0, B11 - 0.1) \quad (1b)$$

$$BLUE = \alpha_1 \cdot B2 \quad (1c)$$

The red and the green bands are mixed with B11 and B12 SWIR bands, in order to enhance the pixel with high temperature. The multiplicative factor α_x is used to adjust the scale of the image and it is set to 2.5. In practice, the infrared bands change the red and green bands, so that the heat information is highlighted and visible to the human eye. In this way it was possible to create a quantitatively correct dataset, since during labeling the eruptions were easily distinguishable from non-eruptions. In Fig. 1 the difference between a simple RGB image and the IR highlighted one is shown.

C. Dataset expansion

More images have been downloaded with the same tool mentioned above in order to fill the no-eruption class. To have an high variability and to reach better results the images have

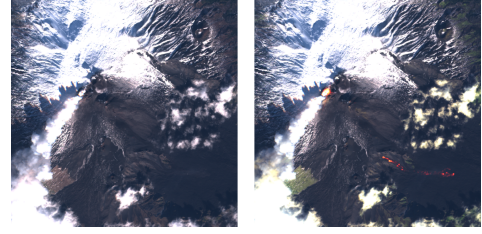


Fig. 1: True RGB color image (left) VS IR highlighted image (right)

been downloaded by focusing on five classes: 1) non-erupting volcanoes, 2) cities, 3) mountains, 4) cloudy images and 5) completely random images. The presence of cloudy images is really important, in order to make the CNN learn to distinguish from eruption smoke and clouds that have their proper shapes, as shown in Figure 2.

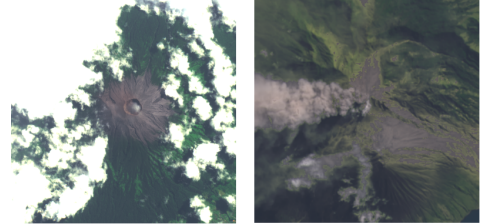


Fig. 2: Volcano surrounded by clouds (left) VS Eruption smoke (right)

The same pre-processing was applied to the new data, since in deep learning context an homogeneous dataset is preferable due to the high sensitivity to variations in the distribution of the input data [10], [11]. The final dataset contains 260 images for the class eruption and 1500 for the class non-eruption. Due to the type of event analyzed, the dataset appears to be unbalanced, indeed an acquisition with an eruption is a rare event. The problem of the imbalanced dataset is addressed in the next sections. A sample from the dataset is shown in Figure 3.

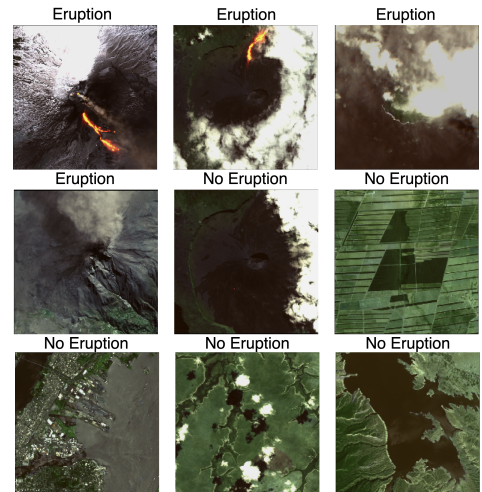


Fig. 3: A set of 9 images from the dataset

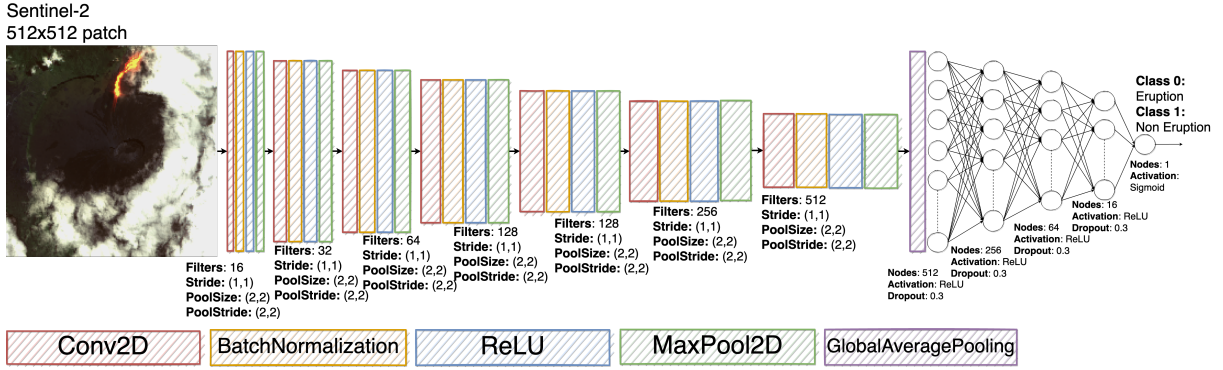


Fig. 4: Network architecture

III. PROPOSED MODEL

The detection task has been addressed, by implementing a binary classifier: the first class is for the eruptions and a second class for the other scenarios. The overall CNN architecture is shown in Figure 4. The proposed CNN can be divided in two sub-network: the convolutional network is responsible of features extraction and the fully connected network is responsible for the classification [10]–[12].

The first sub-network consists of seven convolutional layers, followed by Batch Normalization layers, the ReLU activation function, a pooling layer. Each convolutional layer has a stride value equal to (1,1) and a increasing number of filters. Each maxpooling layer with kernel size and stride of (2,2) halves the feature map. The second sub-network consists of five layers, each layer is followed by the ReLU activation function and a Dropout layer. Also in this case the elements of each layer decrease. In the proposed architecture the Flatten layer, that connects the two sub-netwrok, has been replaced with the Global Average Pooling layer, that drastically reduces the number of trainable parameters and so speeds up the training process.

A. Image Loader

Given the nature of the analyzed hazard, he dataset results unbalanced. An unbalanced dataset, with a number of examples of one class greater than the other, will lead the model to recognise only the dominant class. To solve this issue an arbitrary function called Image Loader from the Phi-Lab *ai4eo.preprocessing* library has been used [13].

This library allows you to define a much more efficient image loader than the already existing Keras version. Furthermore it is possible to implement a data augmentator that allows to define further transformations. The most powerful feature of this library is the one related to the balancing of the dataset through the oversampling technique.

B. Training

During the training phase, for each epoch (lasting about 370 seconds) the error between the real output and the prediction is calculated both on the training dataset and on the validation dataset. The metric used for the error is the accuracy (that works precisely only if there is an equal number of samples

belonging to both classes). The model has been trained for 100 epochs, using the Adam optimizer and the Binary Cross-entropy as loss function.

The training dataset is composed of 1215 examples, of which 334 are with eruptions and 818 are without eruptions. The validation dataset contains 75 eruption samples and 94 no eruption images. Both datasets are subjected to the data augmentation and to the addition of noise to increase the robustness of the model and to solve the spectral diversity between Sentinel-2 and Landsat-7.

The model was trained on the Google Colaboratory platform, where each user can use: 1) GPU1 xTesla K80 , having 2496 CUDA cores, compute 3.7, 12G GDDR5 VRAM, 2) a CPU 1xsingle core hyper threaded i.e (1 core, 2 threads) Xeon Processors @2.3 Ghz (No Turbo Boost), 3) 45MB Cache, 4) 12.6 GB of available RAM and 5) 320 GB of available disk. The trends of the training and the validation accuracy are shown in Fig. 5.

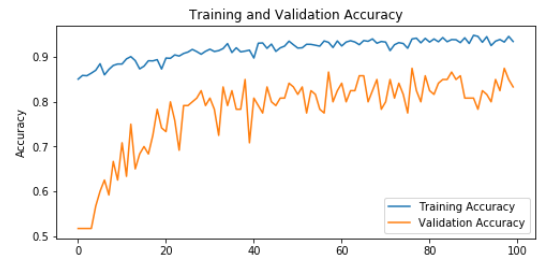


Fig. 5: Training and validation accuracy for the proposed model

The models performances have been computed on the testing dataset. In Figure 6 18 samples are shown, while in Table IV the corresponding ground truth and prediction labels are reported. A low value of predicted label, indicates a low probability of eruption, so the image is classified as no eruption; a high value of predicted label, indicates a high probability of eruption, so the image is classified as eruption; a value next to 0.5 indicates a random prediction.

C. Model Pruning

Since the proposed model have to be uploaded on an on-board system, after the creation of a good detection model,

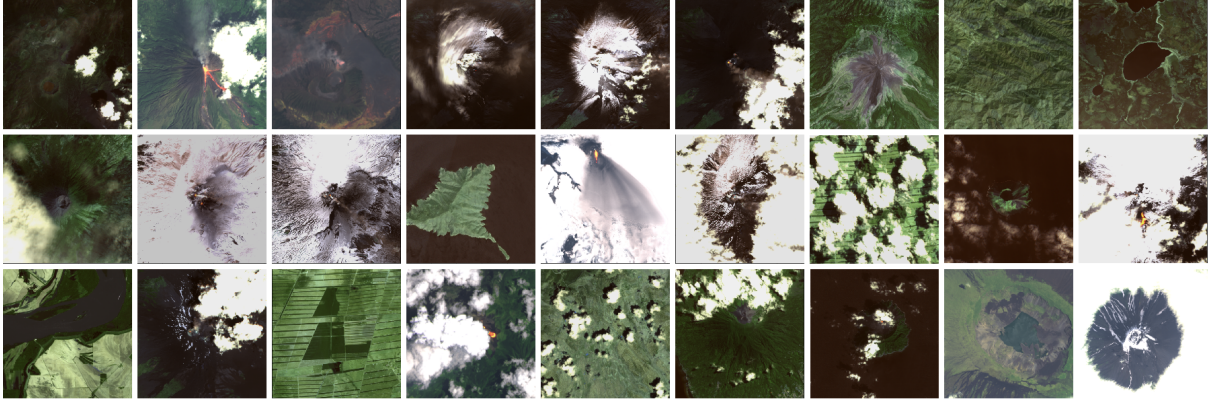


Fig. 6: Sample from the testing dataset

	Row 1		Row 2		Row 2		Row 2		Row 2		Row 2		Row 2		Row 2	
	Ground truth	Predicted	Ground truth	Predicted	Ground truth	Predicted	Ground truth	Predicted	Ground truth	Predicted	Ground truth	Predicted	Ground truth	Predicted	Ground truth	Predicted
Column 1	1.00	0.13	1.00	0.99	1.00	0.99	1.00	0.95	1.00	0.98	1.00	0.99	0.00	0.00	0.00	0.00
Column 2	0.00	0.03	1.00	0.99	1.00	0.99	0.00	0.00	1.00	0.99	1.00	0.99	0.00	0.00	0.00	0.26
Column 3	0.00	0.00	1.00	0.99	0.00	0.00	1.00	0.99	0.00	0.00	0.00	0.02	1.00	0.99	0.00	0.88

TABLE IV: Model results on testing dataset

its optimization in terms of network complexity, number of parameters and execution time to make a new prediction, becomes necessary. These specifics have acquired a great importance for the further objectives of incoming research and its future perspectives: the idea of executing a classification model on a small chip, bonded to the elaboration power of the chip itself, and the on-board computer.

A smaller net was built by pruning the proposed model, the convolutional sub-network has been reduced by removing three layers and the fully connected sub-network has been drastically reduced to two layers. At the cost of greater instability, the new network is still able to discriminate or classify data correctly most of the times. All changes are implemented in order to reduce the number of network parameters: the faster the model, the faster the acquisition and the processing of the images.

The small model has been trained with the same configuration of the original model. The trends of the training and the validation loss and accuracy functions are shown in Fig. 8.

Also in this case the performances have been computed on the test dataset. The same samples shown in Figure 6 have been used to make the comparison with the original model. Table IV shows the results.

The confusion matrix and the model speed, for the two models, are reported in Table VI, where is evident that the performances in terms of good prediction are slightly changed after the model pruning, but the most important aspect is that the images per second that the model and the hardware can handle is increased from 1 to 7. In the next section the hardware setup will be explained.

IV. ON-BOARD VOLCANIC ERUPTION CLASSIFICATION

The proposed models have been used for the on-board volcanic eruption classification. The prototype, mounted on a drone, is composed of a Raspberry PI, a PI camera and a Movidius Stick as shown in Figure 9. The drone systems are independent from the acquisition and classification systems.

The Raspberry PI, with the Raspbian Operating System (OS), is the on-board computer that process the images acquired through the PI camera and sends them to the Movidius Stick, loaded with the CNNs, for the classification. It is also responsible for sending the prediction results to the local PC through the Wi-Fi.

A. Raspberry PI

The Raspberry adopted for this used case is the model Raspberry Pi 3 Model B, the earliest model of the third-generation Raspberry Pi. Table VII shows its main specifications.

B. Camera

The Raspberry Pi Camera Module v2, is a high quality 8 megapixel Sony IMX219 image sensor custom designed add-on board for Raspberry Pi, featuring a fixed focus lens. It is capable of 3280x2464 pixel static images, and supports 1080p30, 720p60 and 640x480p90 video.

The camera can be plugged using the dedicated socket and CSI interface. The main specifications for PI camera are listed in Table VIII.

C. Movidius Stick

The Intel Movidius Neural Compute Stick is a small fanless deep learning USB drive designed to learn AI programming. The stick is powered by the low power high performance Movidius Visual Processing Unit. The main specifications are:

- Supporting CNN profiling, prototyping and tuning workflow
- Real-time on device inference (Cloud connectivity not required)
- Features the Movidius Vision Processing Unit with energy-efficient CNN processing
- All data and power provided over a single USB type A port

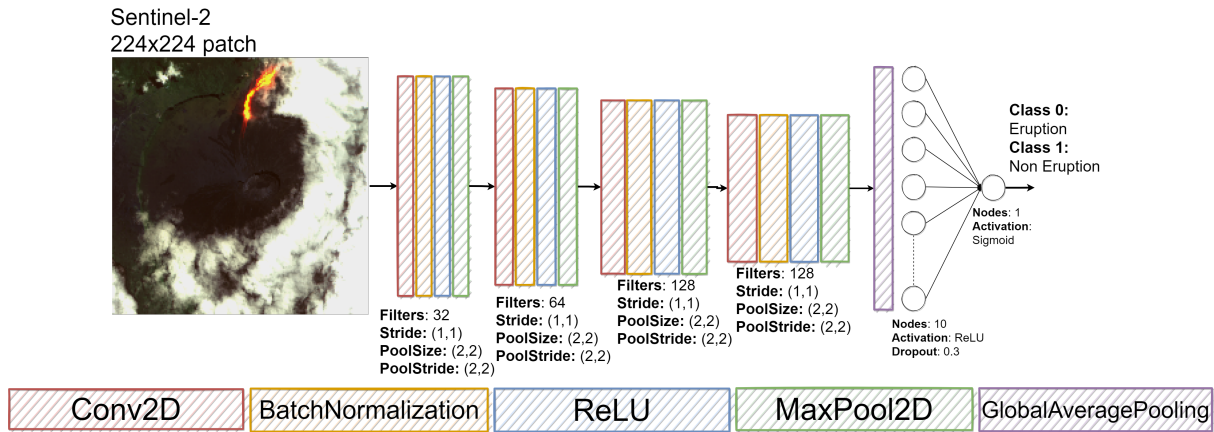


Fig. 7: Smaller Network Architecture

	Row 1		Row 2		Row 2		Row 2		Row 2		Row 2		Row 2		Row 2			
	Ground truth	Predicted	Ground truth	Predicted	Ground truth	Predicted	Ground truth	Predicted	Ground truth	Predicted	Ground truth	Predicted	Ground truth	Predicted	Ground truth	Predicted		
Column 1	1.00	0.99	1.00	0.99	1.00	0.99	1.00	0.01	1.00	0.99	1.00	0.97	0.00	0.00	0.00	0.99	0.00	0.00
Column 2	0.00	0.56	1.00	0.94	1.00	0.97	0.00	0.01	1.00	0.99	1.00	0.99	0.00	0.99	0.00	0.00	1.00	0.00
Column 3	0.00	0.08	0.00	0.00	0.00	0.01	0.00	0.64	0.00	0.00	1.00	0.97	1.00	0.00	0.00	0.00	0.00	0.00

TABLE V: Small Model results on testing dataset



Fig. 8: Training and validation accuracy for the proposed reduced model

Score	Big Model	Small Model
True Positive	0.85	0.83
True Negative	0.85	0.83
False Positive	0.15	0.17
False Negative	0.15	0.17
images/second	1	7

TABLE VI: Bis VS Small Model

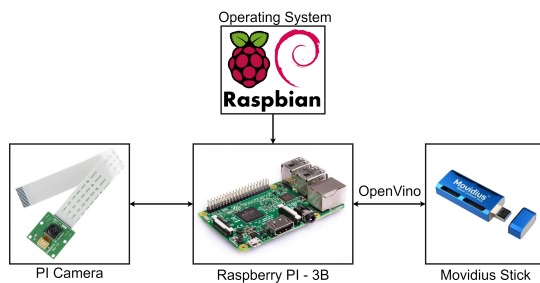


Fig. 9: Schematic for the prototype

- Run multiple devices on the same platform to scale performance

Component	Specifications
Processor	Quad Core 1.2GHz Broadcom BCM2837 64bit CPU 1GB RAM
Wireless systems	BCM43438 wireless LAN and Bluetooth Low Energy (BLE) on board
Hardware systems	100 Base Ethernet
Hardware connectors	40-pin extended GPIO
USB Ports	4 USB 2.0 ports
Video Ports (1)	4 Pole stereo output and composite video port
Video Ports (2)	Full size HDMI
Camera Port	CSI camera port for connecting a Raspberry Pi camera
Display Port	DSI display port for connecting a Raspberry Pi touchscreen display
External Memory Port	Micro SD port for loading your operating system and storing data
Power Supply Port	Upgraded switched Micro USB power source up to 2.5A

TABLE VII: Raspberry PI 3 specifications

Component	Specifications
Focus	Fixed focus lens on-board
Resolution	8 megapixel native resolution sensor
Frame size	3280 x 2464 pixel static images
Video Support	Supports 1080p30, 720p60 and 640x480p90 video
Physical Dimension	Size 25mm x 23mm x 9mm
Weights	Weight just over 3g

TABLE VIII: Raspberry Pi RGB camera specifications

D. Implementation on Raspberry and Movidius Stick

In order to run the experiments with the Raspberry PI and the Movidius Stick, two preliminary steps are necessary: 1) the CNN must be converted from the original format (e.g. Keras model) to an OpenVino format, using the OpenVino library; 2) an appropriate operating system must be installed on the Raspberry (e.g. the Raspbian OS through the NOOBS installer). The implementation process is schematized in Figure 10.

1) *OpenVINO library*: For deep learning, the current Raspberry PI hardware is inherently resource constrained. The Movidius Stick allows faster inference with the deep learning coprocessor that is plugged into the USB socket. In order to transfer the CNN on the Movidius, the network should be optimized, using the OpenVINO Intel library for hardware optimized computer vision.

OpenVINO is extremely simple to use, after setting the

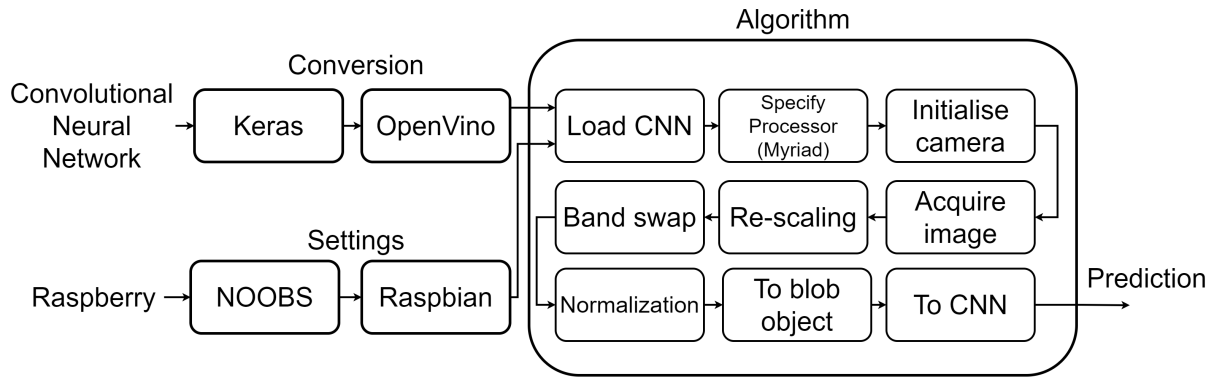


Fig. 10: Block diagram for the implementation on Raspberry and Movidius stick



Fig. 11: Sentinel-2 printed image for on-board models evaluation

the target processor, the OpenVINO-optimized OpenCV can handle the rest. The OpenVINO toolkit is an Intel Distribution. Based on CNN, the toolkit extends workloads across Intel hardware (including accelerators) and maximizes performance:

- enables deep learning inference at the edge
- supports heterogeneous execution across computer vision accelerators (e.g. CPU, GPU, Intel Movidius Neural Compute Stick, and FPGA) using a common API
- speeds up time to market via a library of functions and pre-optimized kernels
- includes optimized calls for OpenCV

After implementation on Raspberry and Movidius, the models were tested by acquiring images using a drone flying over a print made with Sentinel-2 data of an erupting volcano, as shown in Figure 11.

V. CONCLUSIONS

This work aimed to present a first workflow on how to develop and implement an AI model to be suitable for being carried on-board. In particular, the authors developed two detectors of volcanic eruptions. The possibility to produce alerts on-board of a satellite can drastically reduce the time between the image acquisition and the analysis, completely deleting the time for downlinking and other causes of latency.

The authors completed their study with a prototype and a simulation, keeping a low-cost kind of implementation. With commercial and ready-to-use hardware components and a drone, they managed to complete the experiment and to prove their development chain.

ACKNOWLEDGMENT

The research work published in this manuscript has been developed in collaboration with the European Space Agency

(ESA) Φ -lab [14] during the traineeship of Maria Pia Del Rosso and Alessandro Sebastianelli started in 2019. The results achieved for the classification of volcanic eruptions could be suitable for future missions of the ϕ – sat program that represents the first experiment carried out by ESA to demonstrate how AI on-board the satellites can be used for Earth Observation [2].

REFERENCES

- [1] M. P. Del Rosso, A. Sebastianelli, and S. L. Ullo, *Artificial Intelligence Applied to Satellite-based Remote Sensing Data for Earth Observation*. Published by The Institution of Engineering and Technology (IET), 2021.
- [2] European Space Agency (ESA), “ Φ -sat Artificial Intelligence for Earth Observation,” https://www.esa.int/Applications/Observing_the_Earth/Ph-sat, accessed: 2021-06-24.
- [3] M. Titos, A. Bueno, L. Garcia, and C. Benitez, “A deep neural networks approach to automatic recognition systems for volcano-seismic events,” *IEEE Journal of Selected Topics in Applied Earth Observations and Remote Sensing*, vol. 11, no. 5, pp. 1533–1544, 2018.
- [4] N. Anantrasirichai, F. Albino, P. Hill, D. Bull, and J. Biggs, “Detecting volcano deformation in insar using deep learning,” *arXiv e-prints*, pp. arXiv–1803, 2018.
- [5] N. Anantrasirichai, J. Biggs, F. Albino, and D. Bull, “A deep learning approach to detecting volcano deformation from satellite imagery using synthetic datasets,” *Remote Sensing of Environment*, vol. 230, p. 111179, 2019.
- [6] J. Sun, C. Wauthier, K. Stephens, M. Gervais, G. Cervone, P. La Femina, and M. Higgins, “Automatic detection of volcanic surface deformation using deep learning,” *Journal of Geophysical Research: Solid Earth*, vol. 125, no. 9, p. e2020JB019840, 2020.
- [7] “Volcanoes of the World, Smithsonian Institution, National Museum of Natural History, Global Volcanism Program,” http://volcano.si.edu/database/search_eruption_results.cfm, accessed: 2021-06-24.
- [8] Sebastianelli, Alessandro and Del Rosso, Maria Pia and Ullo, Silvia Liberata, “Automatic Dataset Builder for Machine Learning Applications to Satellite Imagery,” *Elsevier Software-X*, 2021.

- [9] N. Gorelick, M. Hancher, M. Dixon, S. Ilyushchenko, D. Thau, and R. Moore, "Google earth engine: Planetary-scale geospatial analysis for everyone," *Remote Sensing of Environment*, 2017. [Online]. Available: <https://doi.org/10.1016/j.rse.2017.06.031>
- [10] Y. LeCun, Y. Bengio, and G. Hinton, "Deep learning," *nature*, vol. 521, no. 7553, pp. 436–444, 2015.
- [11] I. Goodfellow, Y. Bengio, A. Courville, and Y. Bengio, *Deep learning*. MIT press Cambridge, 2016, vol. 1, no. 2.
- [12] Kim, Phil, "Convolutional neural network," in *MATLAB deep learning*. Springer, 2017, pp. 121–147.
- [13] ESA Φ -lab, "Ai4eo git-hub page." <https://github.com/ESA-PhiLab/ai4eo>, accessed: 2021-06-24.
- [14] European Space Agency (ESA), " Φ -lab," <https://philab.phi.esa.int/>, accessed: 2021-06-24.